Theoretical and Applied Climatology (2023) 153:1085–1103
https://doi.org/10.1007/s00704-023-04531-z

RESEARCH

Validation of CYGNSS soil moisture products using in situ measurements: a case study of Southern China

Zhounan Dong[1,2] · Shuanggen Jin[3,4] · Li Li[1,2] · Peng Wang[1]

Received: 19 December 2022 / Accepted: 5 June 2023 / Published online: 12 June 2023

Abstract

The spaceborne Global Navigation Satellite System-Reflectometry (GNSS-R) has proven its worth in terrestrial remote sensing applications. Its application to detecting land surface soil moisture (SSM) is particularly intriguing, as it can provide fine-scale SSM products to supplement traditional satellite-based active and passive missions. Various retrieval algorithms have been developed to produce SSM products using spaceborne GNSS-R. However, detailed evaluations of product reliability and robustness are still absent. In this study, we used three data sources to evaluate the level-3 SSM products from the CYclone Global Navigation Satellite System (CYGNSS) mission: (1) satellite-based microwave radiometry product from Soil Moisture Active and Passive (SMAP) mission; (2) a model-based product of Modern-Era Retrospective analysis for Research and Applications; and (3) in situ measurements from over 1800 ground stations in the Chinese soil moisture monitoring network. The study uses typical relative skill metrics and triple collocation approach (TCA)-based metrics, along with corresponding confidence intervals, to analyze the performance of SSM products derived from CYGNSS observations. According to the pixel-by-pixel validation and overall statistical findings, the results reveal that the current CYGNSS-based SSM exhibits low performance in southern China when compared to the radiometry-based data. The coefficient of determination (R^2) is low (median R^2=0.088) and the unbiased root-mean-square-difference (ubRMSD) is 0.057 cm^3cm^{-3}, which is poorer than the results from SMAP against in situ measurements (median R^2=0.25, ubRMSD=0.046 cm^3cm^{-3}). The TCA-based analysis also revealed that CYGNSS had a relatively poor performance, with the lowest median R^2 value of 0.167 and the largest median error standard deviation (ESD) value of 0.055 cm^3cm^{-3}. To obtain improved results that can better support related operational applications in the future, enhanced retrieval algorithms and high-accuracy calibration referenced data must be utilized.

1 Introduction

Soil moisture is an important indicator of global climate change and has been identified as one of the essential climate variables (Wagner et al. 2012). Continuous collection of large-scale and long-term soil moisture data is essential for geoscience research and agricultural production (Vreugdenhil et al. 2022). Geoscientists are particularly interested in surface soil moisture (SSM) remote sensing using active and passive microwave sensors. Theoretical and validation experiments have demonstrated that L-band microwaves, which are sensitive to soil moisture changes, less vulnerable to vegetation, and unaffected by clouds, are optimal for SSM remote sensing (Saeedi et al. 2021). The Soil Moisture and Ocean Salinity (SMOS) mission (Kerr et al. 2010) and the Soil Moisture Active and Passive (SMAP) mission (Entekhabi et al. 2010) are two dedicated satellite missions for global-scale SSM remote sensing. These missions have been equipped with L-band monostatic microwave radiometers, offering a good perspective on monitoring global SSM dynamics.

The advancement of the Global Navigation Satellite System (GNSS) has facilitated the development of the spaceborne GNSS-Reflectometry (GNSS-R) technique (Martin-Neira

✉ Zhounan Dong
zndong@mail.usts.edu.cn

1 School of Geography Science and Geomatics Engineering, Suzhou University of Science and Technology, 99 Xuefu Road, Suzhou 215009, China

2 Research Center of Beidou Navigation and Environmental Remote Sensing, Suzhou University of Science and Technology, 99 Xuefu Road, Suzhou 215009, China

3 School of Surveying and Land Information Engineering, Henan Polytechnic University, Jiaozuo 454000, China

4 Shanghai Astronomical Observatory, Chinese Academy of Sciences, 80 Nandan Road, Shanghai 200030, China

et al. 2001). GNSS-R receiver receives the opportunity signal, which is transmitted by the GNSS satellite and reflected off the Earth's surface, forming a bistatic (multi-static) forward scattering radar (Gleason et al. 2005). The properties of the scattering interface, which are characterized by geophysical parameters, affect the echo in form and reflected power. The fundamental basis of the GNSS-R technique is mapping the features derived from the distorted observations to the interested geophysical parameters. The small size and mass of the GNSS-R receiver make it easily deployable on the micro-satellite platform with lower power dissipation (Ruf et al. 2012) and easily develop low Earth orbit observing constellation, which can help fill spatial-temporal gaps in dedicated SSM remote sensing satellite observations. Therefore, leveraging spaceborne GNSS-R technique allows for the collection of high spatiotemporal resolution SSM information across large regions.

The SSM products are derived from satellite-based passive microwave radiometry sensors with coarse spatial resolutions ranging from 25 to 50 km (Gelaro et al. 2017; Chew and Small 2020). Many studies have focused on comparing the accuracy of these satellite estimates to ground-based measurements, which represent the most prevalent approach employed in performance validation studies. Measurements from in situ soil moisture stations can only represent soil wet conditions within a few hundred meters surrounding the station. The application of site measurements is primarily limited by their quantity and observation extent. Therefore, dense core validation sites and sparse in situ networks are typically used to assess the quality of coarse-resolution satellite-based products. The results of these assessments are considered more reliable and can provide the most precise evaluation (Peischl et al. 2012; Colliander et al. 2022), despite the large differences in spatial resolution between the ground station and the coarse satellite-based products. Based on the previous study, the point-scale SSM data from in situ measurements can be indicative of a large area based on the temporal stability concept (Brocca et al. 2011), which implies that ground probe observations can be a good benchmark for satellite-based product validation. Additionally, nearest-neighbor (NN) searches are commonly employed to match station measurements from sparse networks with the referenced grid for satellite-based products (Gruber et al. 2020). Many studies have utilized diverse comparison approaches to evaluate different satellite-derived SSM datasets across various regions and scales (Cui et al. 2017; Chen et al. 2018; Wang et al. 2021).

The CYclone Global Navigation Satellite System (CYGNSS) mission has emerged as a highly valuable data source for satellite-based GNSS-R SSM retrieval. Despite being originally designed for ocean surface wind speed monitoring (Clarizia and Ruf 2016), the CYGNSS mission also offers significant advantages for SSM retrieval, including near-daily revisit time and the enormous amount of freely available data. Previous studies mainly focus on SSM retrieval algorithm development and the model performance assessment based on the GNSS-R technique (Chew and Small 2018; Al-Khaldi et al. 2019; Clarizia et al. 2019; Yan et al. 2020). The semi-empirical models commonly employed rely on establishing a linear mapping relationship between aggregated observables obtained from GNSS-R observations and reference SSM for individual grid cells. The University Corporation for Atmospheric Research (UCAR) and the University of Colorado at Boulder (CU) investigators have published their estimated daily SSM products using CYGNSS data at the Physical Oceanography Distributed Active Archive Center (PODAAC). These products were generated using an empirical linear regression inversion algorithm, accompanied by a series of well-established and rigorous pre-processing procedures (Chew and Small 2020). Machine learning and artificial neural networks can handle complex and non-linear relationships between GNSS-R observables and SSM. They can accurately capture the intricate relationships present in the data, integrate diverse data sources, adapt to different conditions, and efficiently automate processing. This makes them a valuable approach for advancing soil moisture remote sensing capabilities with GNSS-R (Eroglu et al. 2019; Jia et al. 2021). However, the calibration of GNSS-R observables to SSM in nearly all retrieval algorithms predominantly relies on SSM products provided by the SMAP mission. Furthermore, the evaluation of retrieval performance often utilizes in situ measurements from the International Soil Moisture Network (ISMN), which are mainly located in the USA and Europe. The performance in other regions, especially in China, has not been reported to date (Chew and Small 2020; Wan et al. 2022).

There is a lack of consensus regarding the accuracy of the terrestrial SSM estimation through CYGNSS observations. Various spatial and temporal factors, such as the choice of study area, the study period, reference data, and auxiliary data employed, as well as the data pre-processing and evaluation strategies adopted, collectively impact the overall quality of inversion results. Accurate evaluation of the quality of satellite-based microwave remote sensing products is essential to understand the spatial and temporal distribution of uncertainty before utilizing them in other geoscience disciplines. While reliable validation frameworks and methods have been proposed for evaluating satellite-based active and passive microwave product evaluation (Gruber et al. 2020), few GNSS-R SSM assessment studies follow the same rigorous approach as other satellite-based data. These studies utilize high-quality reference data sets and employ the triple collocation approach (TCA) to obtain robust uncertainty metrics, along with estimated confidence

intervals. Overall, the current CYGNSS-derived SSM still lacks robust assessment.

This study aims to comprehensively assess the CYGNSS-derived SSM products, providing insights into the current performance of spaceborne GNSS-R in monitoring SSM and offering a guide for future algorithm development and related applications. The methodology followed in this work adheres to the good practice guidelines outlined in Gruber et al. (2020) and was implemented in Southern China using various SSM data sources from the year 2018. The remaining part of the paper proceeds as follows: the second section introduces the data collection and methodology used in the study. The validation findings are presented in the third part. The discussions are given in section 4. The final section provides a concise overview of the research.

2 Materials and methods

2.1 Datasets

2.1.1 CYGNSS

The primary objective of the CYGNSS mission was to collect sea surface wind speeds with high spatial and temporal resolution, specifically for studying tropical cyclone intensity. The space segment of CYGNSS mission consists of eight small satellites orbiting on a plane, covering a latitude range of 38° north and south. Meanwhile, the observing system can provide observable of reflectivity over the land surface that can further be used for SSM retrieval (Dong and Jin 2021). The mission science teams have released various levels of data products to facilitate relevant scientific studies and operational applications. UCAR/CU has developed CYGNSS L3 volumetric SSM products with a spatial resolution of 36 km by 36 km and daily/sub-daily temporal resolution (https://podaac.jpl.nasa.gov/dataset/CYGNSS_L3_SOIL_MOISTURE_V1.0). A specific SSM retrieval algorithm was designed for CYGNSS observations, in which the CYGNSS-derived reflectivity was calibrated to SSM using a pre-generated semi-empirical linear model at each the Equal-Area Scalable Earth (EASE) Grid-2 grid pixel. This algorithm employs SMAP mission provided SSM products as the surface reference values (Chew and Small 2020). In this study, we focus on evaluating the daily SSM parameter from the L3 product.

2.1.2 SMAP

The SMAP mission was primarily designed to collect continuous global-scale SSM data at hydrometeorology and hydroclimatology scales, with a temporal frequency of every 2–3 days. The sensors on board SMAP satellite consist of a high-resolution active radar and passive radiometer sharing a single feedhorn and parabolic reflector at L-band frequency. However, due to a power amplifier malfunction, the radar component failed after launch. Consequently, the available dataset for SSM estimation is limited to radiometry measurements. In this study, the SMAP L3 V8 products (SPL3SMP) were used (https://nsidc.org/data/spl3smp/versions/8). The baseline algorithm for SSM retrieval has been updated from the previous single channel algorithm-vertical polarization to the dual channel algorithm, which has shown slightly improved performance in validation over certain agricultural cropland core sites (ONeill, Peggy E. et al. 2021). The passive radiometer operates at a spatial resolution of 40 km, and the SSM is retrieved and sampled on the 36 km×36 km EASE-Grid2 grid cell. The daily updated HDF5 file contains each half-orbit pass of the satellite, namely descending and ascending passes, respectively. Considering that the adopted model-based surface temperature parameter used in the retrieval algorithm exhibits greater uniform in two-dimensional planes and vertical profiles in the morning, resulting in better data quality for the descending half-orbit pass of the satellite (Chen et al. 2018), only the recommended AM data are used in this study.

2.1.3 Soil sparse network

Automatic soil moisture in situ stations are renowned for their high measurement accuracy and ability to provide continuous monitoring at various depths. Therefore, the in situ station measurements are widely accepted as the reference values for the satellite-based SSM product evaluation. In this study, raw hourly soil moisture measurement data set were collected from the Chinese soil moisture monitoring network in the year of 2018. The soil moisture network includes over 2000 stations equipped with frequency domain reflectometry sensors, enabling the measurement of volumetric SSM at different depths (Wu et al. 2016). These measurements were recorded as average values during the 10 min leading up to each hourly interval. SSM values at a depth of 0–10 cm were selected for this study. Figure 1 illustrates the distribution of these selected stations across China. Within the scope of the CYGNSS constellation and to meet the requirement of data quality control, a total of 1824 stations are qualified and used for validation purposes. As the collected raw data set did not undergo quality control processing, the measured SSM time series may contain outlies resulting from instrument abnormalities. To enhance the quality of the in situ measurements, the preprocessing approach outlined in Saeedi et al. (2021) is employed. This approach utilized the median absolute deviation (MAD) method to detect and remove the outliers to improve the quality of in situ measurements:

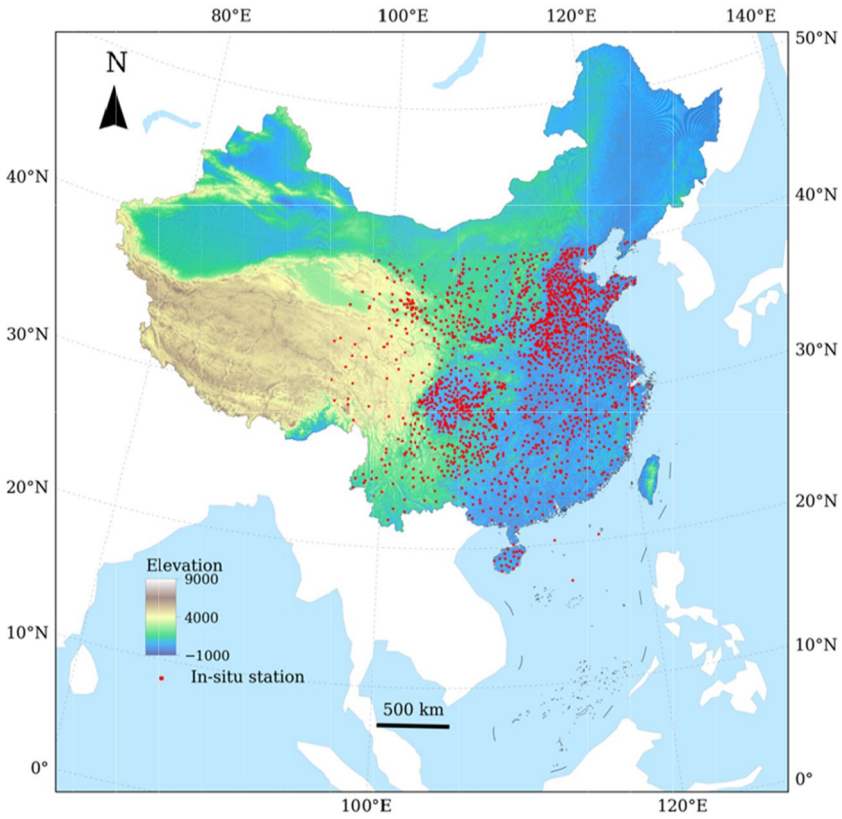

Fig. 1 Geographical distribution of selected in situ stations from the Chinese soil moisture monitoring network for evaluation purposes

$$\begin{cases} \text{Median}(X) - \beta \times \text{MAD}(X) < X_i < \text{Median}(X) + \beta \times \text{MAD}(X) \\ \text{MAD}(X) = b \times \text{Median}\left(\left|X_i - \text{Median}(X)\right|\right) \\ b = \begin{cases} 1.4826, X \sim N\left(\mu, \sigma^2\right) \\ \frac{1}{Q(0.75)}, \text{other} \end{cases} \end{cases} \tag{1}$$

where X represents the time series at each in situ station, X_i denotes the *i*th sample, and the value of b is determined based on the distribution of time, with β being a scale factor that can use to adjust the conservativeness of rejection criterion. In this study, β is set to 2.5. The normality of the time series is tested using D'Agostino and Pearson's test (D'Agostino 1971; D'Agostino and Pearson 1973), which combines skewness and kurtosis to provide an omnibus normality test, Q(0.75) represents the 0.75 quantiles.

2.1.4 MERRA-2

The model-based data set of the Modern-Era Retrospective analysis for Research and Applications, Version 2 (MERRA-2; Gelaro et al. 2017) is the latest atmospheric reanalysis generated by NASA's Global Modelling and Assimilation Office. The land SSM information is included in "MERRA-2 tavg1_2d_lnd_Nx" file collection. This collection offers global 1-hourly estimates of land SSM parameters with a spatial resolution approximately 50 km in the latitudinal direction, represented on 0.5° × 0.625° grid, spanning from 1980 to present (M2T1NXLND) (Reichle et al. 2017). The SSM values in this dataset correspond to a depth of 0–5 cm and are assimilated using multiple observations (https://disc.gsfc.nasa.gov/datasets/M2T1NXLND_5.12.4/summary). For more detailed information, please refer to Gelaro et al. 2017.

2.2 Methodology

2.2.1 Pre-processing

The preprocessing technique for satellite-based remote sensing product assessment typically involves four key processes: data masking, spatial and temporal collocation, decomposition, and rescaling (Gruber et al. 2020). The CYGNSS L3 SSM product released by UCAR/CU has undergone masking to exclude the unreliable area, such as inland water bodies and rainforests. Additionally, due to the low signal-to-noise ratio of CYGNSS observations in the Tibetan Plateau in China, which can be influenced by factors such as snow, permafrost, and topography effect, data across this region were also excluded from the product. The quality control strategy for in situ measurements has been mentioned before. High-uncertainty SSM values in SMAP and MERRA-2 products are also masked out, following the recommendations of the data providers. It should be noted

that the temporal coverage of this study is limited to 2018, as only in situ measurements during this period of time were collected. To ensure consistency with CYGNSS data, the in situ measurements were upscaled to match the temporal resolution of CYGNSS SSM data by using the average value. Firstly, the station locations were projected onto the EASE-Grid2 grid. Subsequently, the in situ measurements within the same grid cell were aggregated into daily averages, representing the SSM time series observed at the corresponding grid pixel. During the projection, it was observed that most grid pixels contained only one or two stations as summarized in Table 1. In order to maintain consistency across all grid datasets and ensure spatial and temporal collocation, the MERRA-2 data were also resampled to the 36 km×36 km EASE-Grid2 grid using a nearest-neighbor interpolation approach. Furthermore, the short-term anomalies were computed using a 35-day sliding average window to remove seasonal effects on the collocations (Brocca et al. 2011):

$$SM_{\text{anom}}(t) = \frac{SM(t) - \overline{SM(t-17:t+17)}}{\sigma[SM(t-17:t+17)]} \tag{2}$$

where SM(t) represents the SSM value at an individual sampling epoch of time series, the overbar indicates the temporal average, and σ denotes the standard deviation of the selected series in the average window, which is defined by $t \pm 17$ epochs around the computed epoch.

In the evaluation using the TCA, a rescaling approach was applied to mitigate systematic differences between the satellite-derived and site-specific SSM data. The linear bias correction method, as proposed by Brocca et al. (2010), was utilized to align the temporal mean and standard deviation of data sets.

2.2.2 Performance indicators

The spatial resolution of GNSS-R observations is influenced by a combination of observation geometry and scattering surface characteristics. Additionally, the specular scattering points of spaceborne GNSS-R exhibit a pseudo-random distribution. To improve the signal-to-noise ratio, the CYGNSS observables were commonly gridded using spatial and temporal averaging in the retrieval algorithm. These factors pose challenges in establishing a core validation station for the evaluation of CYGNSS SSM. The accuracy of GNSS-R SSM products can also be verified by employing appropriate data analysis techniques, utilizing station measurements from sparse networks, leveraging products from other satellite remote sensing systems, and surface models.

This study utilizes various skill metrics to assess the agreement among CYGNSS, SMAP, and in situ data. The skill metrics employed include mean bias, unbiased root-mean-square-difference (ubRMSD), correlation coefficients, and triple collocation-based metrics. These metrics provide insights into the level of agreement between the datasets and help evaluate their uncertainty.

Temporal mean bias:

$$bias_{xy} = \frac{1}{N}\sum_{i=1}^{N}\left(x_i - y_i\right) \tag{3}$$

where x_i is the gridded SSM date point to be verified, and y_i is the collocated reference SSM; the size of the samples is denoted by N.

Unbiased root-mean-square-difference:

$$ubRMSD_{xy} = \sqrt{\frac{1}{N}\sum_{i=1}^{N}\left(\left(x_i - \bar{x}\right) - \left(y_i - \bar{y}\right)\right)^2} \tag{4}$$

where $\bar{x}$ and $\bar{y}$ indicate the mean values of the SSM to be validated and the reference SSM time series at the grid cell, respectively.

Pearson correlation coefficient:

$$R_{xy} = \frac{\sum_{i=1}^{N}\left(x_i - \bar{x}\right)\left(y_i - \bar{y}\right)}{\sqrt{\sum_{i=1}^{N}\left(x_i - \bar{x}\right)^2 \sum_{i=1}^{N}\left(y_i - \bar{y}\right)^2}} \tag{5}$$

the correlation coefficient can also be represented as the square of its value, known as the coefficient of determination R^2, which typically ranges from 0 to 1.

However, due to the limited number of samples and presence of sampling errors, there is inherent uncertainty associated with the validation metrics. To quantify this variation, confidence intervals (CIs) are used. A CI represents the range of values within which the point estimate is expected to fall a certain percentage of the time if the experiment is repeated or the population is resampled in the same manner. CIs are useful for conveying the degree of variation around a point estimate (Hazra 2017). The width of CI can vary depending on the confidence level, sample size, and sample variability. A higher sample variability leads to a wider CI. The confidence level, on the other hand, is the proportion of times an estimate can be reproduced between the upper $\upsilon(X)$ and lower limits $\mu(X)$ of the CI for a specific statistical parameter θ.

Table 1 Summary of in situ stations projected to EASE-Grid2 grid located within a same grid pixel

Grid pixel count	637	229	75	37	11	4	1	2	1
Stations	1	2	3	4	5	6	7	8	10

$$\Pr\{\mu(X) < \theta < \upsilon(X)\} = \gamma = 100\% \bullet (1-\alpha) \tag{6}$$

The required confidence level γ is often indicated as one minus the alpha value (α) employed in the statistical test, where the α is the probability threshold for statistical significance.

To void obtaining an extremely broad interval that loses its practical significance, this work utilizes an 80% confidence level for estimating the CI (Gruber et al. 2019, 2020). Additionally, considering that sample auto-correlation can impact the width of the CI, the assumption of first-order auto-regressive AR(1) behavior is made for the time series, the lag-1 auto-correlation was employed to calculate the effective sample size:

$$n_e = n \cdot \frac{1-\sqrt{\rho_x \bullet \rho_y}}{1-\sqrt{\rho_x \bullet \rho_y}} \tag{7}$$

where $\rho_i = e^{-\frac{d_m}{\tau_i}}$, $\mathrm{i} \in [\mathrm{x}, \mathrm{y}]$ is obtained from fitted AR(1) model, τ is the fitted persistence time of time series, and d_m is the median time distance between consecutive valid collocations. Using the values from sample data to replace the population values:

$$CI_{bias_{xy}} = \bar{x} \pm t^* \frac{s}{\sqrt{n}} \tag{8}$$

$$CI_{ubRMSD_{xy}=} \pm s\frac{\sqrt{n-1}}{\chi^*} \tag{9}$$

where $\bar{x}$ is the sample mean, s is the sample standard deviation, t^* is the critical value of the t-distribution, and χ^* is the critical value of the χ-distribution. Check the corresponding look-up table with necessary parameters (alpha value, degrees of freedom) to determine the two-tailed interval.

The calculation of Pearson's correlation coefficient CI involves Fischer's z-transformation, which is used to convert R_{xy} into a new random variable Z_{xy}, that approximately follows a normal distribution $Z_{xy} \sim N\left(0.5\ln\left(\frac{1+R_{xy}}{1-R_{xy}}\right),\ (n-3)^{-0.5}\right)$. Subsequently, when determining the upper and lower bounds of the confidence interval, the reverse transformation is applied on the data.

$$CI_{R_{xy}} = \left[\frac{e^{2z^{1-\alpha}}-1}{e^{2z^{1-\alpha}}+1}, \frac{e^{2z^{\alpha}}-1}{e^{2z^{\alpha}}+1}\right] \tag{10}$$

The CI of the correlation coefficient is simply squared to obtain the CI of the coefficient of determination R^2.

2.2.3 TCA-based metrics

TCA is a widely used statistical approach for estimating random errors in three independent groups of time series that represent different error patterns for the same geophysical variable (Stoffelen 1998). In the context of evaluating different reference datasets, each with its own unknown observation errors, TCA offers a way to integrate these independent data sources and compute their relative errors, without making any assumptions about the specific number of errors. In our case, we denote the three independent time series from different observing systems as X, Y, and Z, while the true value is represented by Θ.

$$\begin{aligned} x &= \alpha_x + \beta_x\Theta + \varepsilon_x \\ y &= \alpha_y + \beta_y\Theta + \varepsilon_y \\ z &= \alpha_z + \beta_z\Theta + \varepsilon_z \end{aligned} \tag{11}$$

where α_i and β_i ($i = x, y, z$) are the first-order additives and second-order multiplicative systematic errors, and ε_i indicates the zero-mean random errors ($\langle\varepsilon_X\rangle = \langle\varepsilon_Y\rangle = \langle\varepsilon_Z\rangle = 0$) of corresponding time series. The estimation of the random error standard deviation (ESD) and correlation coefficient can be calculated using the covariances of the products:

$$\begin{aligned} \sigma_{\varepsilon_X} &= \sqrt{\sigma_X^2 - \frac{\sigma_{XY}\sigma_{XZ}}{\sigma_{YZ}}} \\ \sigma_{\varepsilon_Y} &= \sqrt{\sigma_Y^2 - \frac{\sigma_{YX}\sigma_{YZ}}{\sigma_{XZ}}} \\ \sigma_{\varepsilon_Z} &= \sqrt{\sigma_Z^2 - \frac{\sigma_{ZY}\sigma_{ZX}}{\sigma_{YX}}} \end{aligned} \tag{12}$$

$$\begin{aligned} R_X &= \sqrt{\frac{\sigma_{XY}\sigma_{XZ}}{\sigma_X^2\sigma_{YZ}}} \\ R_Y &= \sqrt{\frac{\sigma_{XY}\sigma_{YZ}}{\sigma_Y^2\sigma_{XZ}}} \\ R_Z &= \sqrt{\frac{\sigma_{XZ}\sigma_{YZ}}{\sigma_Z^2\sigma_{XY}}} \end{aligned} \tag{13}$$

where σ_{ε_X} and R_X are the interested product ESD and correlation coefficient of X, respectively. σ_X^2 indicates the collocated variance of time series X, and σ_{XY}, σ_{XZ}, and σ_{YZ} are the covariance between X and Y, X and Z, and Y and Z, respectively. For the ESD of time series Y and Z, the identifier (notion) items are σ_{ε_Y} and σ_{ε_Z}. The correlation coefficients of Y and Z are identified as R_Y and R_Z, respectively.

Furthermore, it is important to ensure that the sample sequence is sufficiently long for reliable evaluation when calculating TCA-based metrics. Previous studies (Dorigo et al. 2010; An et al. 2016) have recommended a sample size threshold of 100. To enhance the robustness of the estimates, the median of the bootstrapping sampling distribution is preferred over direct estimates (Gruber et al. 2020). This study presents the spatial distribution of the median metric obtained through TCA. Moreover, the CI is directly estimated using bootstrapping as a non-parametric method with at least 1000 re-sampling (Efron and Tibshirani 1986).

2.2.4 Experimental design

The study area is confined to the southern part of the Chinese mainland, specifically below of the 38° latitude excluding the Tibetan Plateau. The temporal coverage encompasses the entirety of the year 2018. The primary objective of this study is to assess of the quality of CYGNSS SSM products. To achieve this, the validation strategy involves computing relative skill metrics by comparing the performance of the CYGNSS data to both the in situ measurements and the SMAP data. TCA is utilized to determining the random errors associated with different datasets. Due to differences in the spatiotemporal coverage of various SSM products, the process of space and time collocation to obtain matched time series results in reduction in the number of data points for each grid cell as more products are included in collocation. For this study, the reference data sources are limited to SMAP, MERRA2, and Chinese ground station measurements. The evaluation of CYGNSS L3 SSM and SMAP L3 SSM datasets involved comparing them with gridded in situ measurements on a daily scale to assess the performance of CYGNSS and SMAP data. It is important to note that the CYGNSS product is calibrated using SMAP data as the land surface reference "true value." The TCA-based analysis requires the error of three SSM datasets to be independent. Therefore, we incorporated MERRA-2 data into the TCA, forming two groups of triples to evaluate the uncertainty associated with the current CYGNSS-based SSM.

3 Results

3.1 Relative evaluation of SSM against ground observations

By leveraging the sparse network of ground SSM monitoring stations in China, the performance of spaceborne GNSS-R estimations can be effectively validated. The high revisit cycle and spatial coverage of CYGNSS enable the generation of relatively continuous time series at evaluated pixel in the study area, which can be compared against station data and SMAP data through space and time collocation processing. After excluding time series with a length of less than 50, the total number of 90723 matching data pairs were obtained for CYGNSS, SMAP, and in situ measurements across all 865 grid cells. Approximately 48% of all valid evaluation pixels in raw time series matches had more than 100 data points. It is important to highlight that the collocations were predominantly determined by the number of in situ stations, given the superior spatial coverage of satellite-based data. Figure 2 illustrates the number of temporal matches and effective sample size with auto-correlation correction for each valid grid pixel. Due to the inherent auto-correlation nature of soil moisture time series, the number of effective data points for CI computation, when considering lag-1 auto-correlation correction, is relatively smaller. Moving forward, we will assess the quality of the CYGNSS-derived soil moisture products based on the matched time series at each grid cell.

Figure 3 illustrates the spatial distribution of the temporal mean bias among the collocated time series derived from CYGNSS, SMAP, and in situ data for each valid grid pixel. Additionally, the difference between the upper and lower confidence limits of the 80% CI is shown to indicate the reliability of bias estimate. Comparing the CYGNSS SSM to the in situ SSM, positive bias values were observed in the east and south regions. This indicates that wetter SSM estimates exist in those areas. Conversely, negative bias values were observed over the western and northern regions of the study area, indicating that CYGNSS tends to provide drier estimates in these areas compared to the in situ SSM. When compared to the in situ data, SMAP generally demonstrates larger SSM values with positive bias values. Notably, the

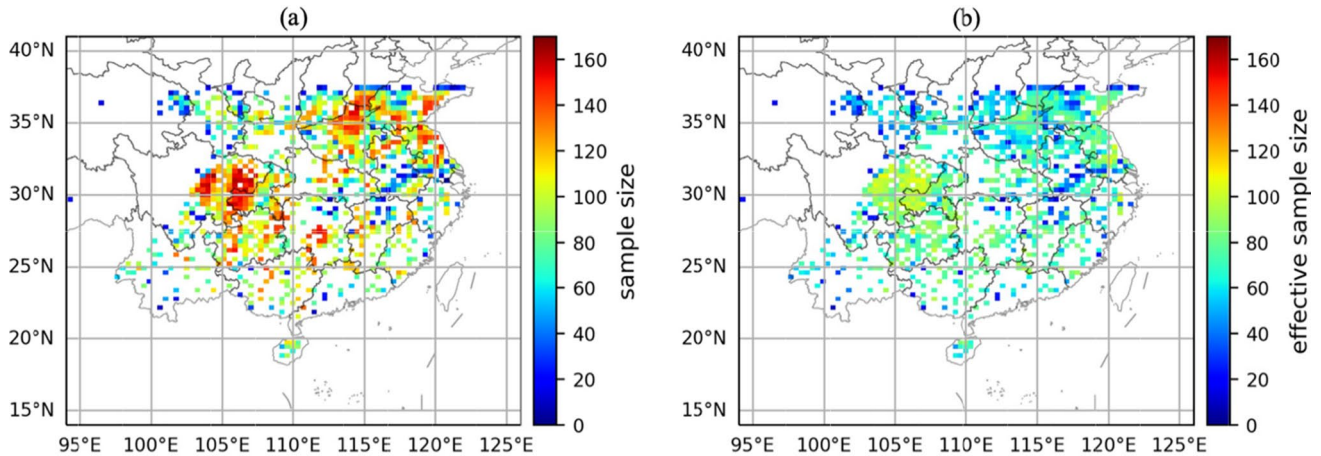

Fig. 2 Temporal matching sample size of CYGNSS, SMAP, and in situ soil moisture samples in each grid cell (**a**), and effective sample size (**b**) accounting for auto-correlation correction in the raw time series during the year 2018

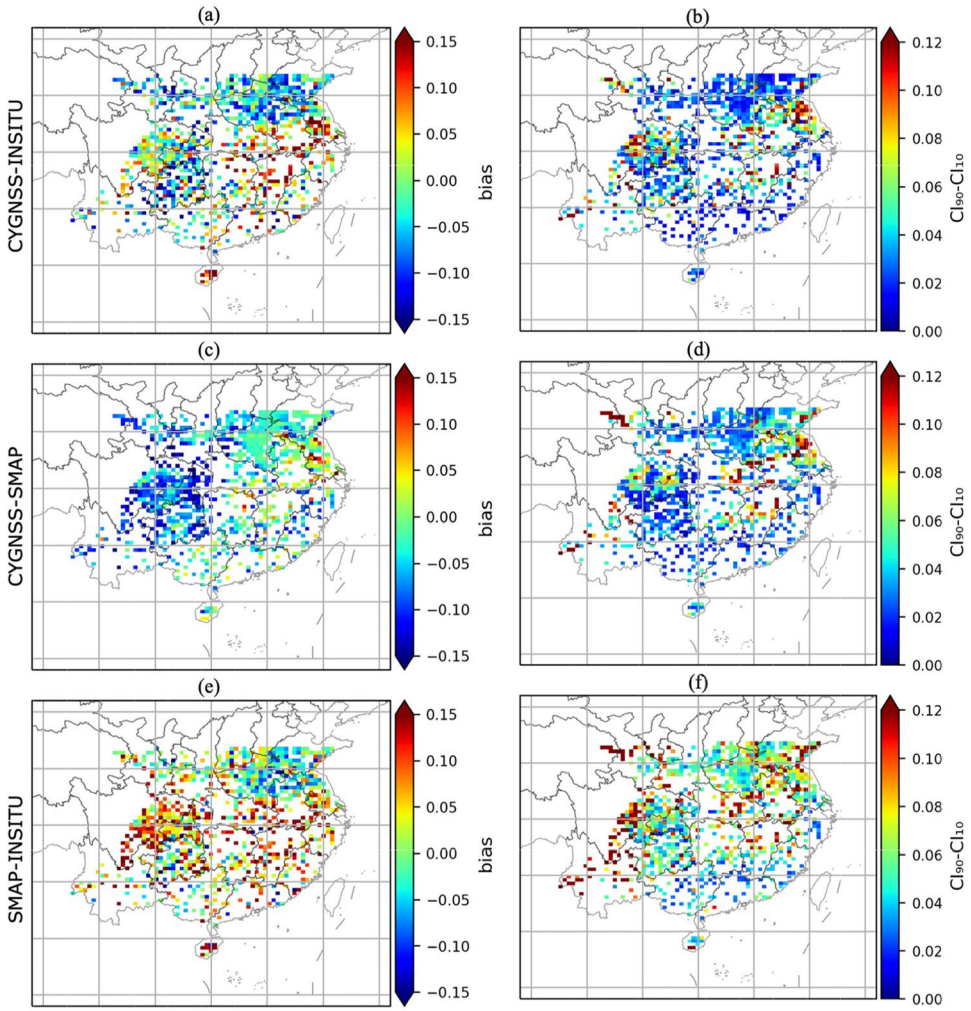

Fig. 3 Temporal mean bias (**a**, **c**, **e**) and corresponding 80% confidence interval (**b**, **d**, **f**) between the raw surface soil moisture time series of CYGNSS, SMAP, and in situ data at collocated grid pixel

spatial distribution pattern of the systematic errors propagated by the SMAP data is followed by the CYGNSS data. The temporal bias of CYGNSS SSM shows values close to zero in the eastern region of 110°E, while negative bias is predominantly observed in the western region of 110°E compared to the SMAP data. The SMAP data tends to exhibit an overestimated trend in most regions when compared to the in situ data, especially in the majority of areas south of Henan Province. However, it shows a positive bias in Henan, northern Anhui, and Shandong Province. Since CYGNSS SSM is derived through direct calibration from surface effective reflectivity using a pre-fitted linear model based on SMAP SSM at each individual pixel, it superimposes the bias of SMAP data when compared to in situ data. As a result, CYGNSS tends to overestimates SSM in areas south of Henan Province and east of 110°E. The spatial distribution of the CI of the estimated mean bias between CYGNSS and in situ, as well as between SMAP and in situ, is generally consistent across most grid cells, with a width of less than 0.02 cm^3cm^{-3} in the majority of cases.

Figure 4 presents the spatial distribution of R^2 between CYGNSS, SMAP, and in situ data at each grid pixel, along with a corresponding 80% CI. Overall, the R^2 values between CYGNSS SSM and in situ measurements are significantly lower in the majority of regions, while the SMAP product demonstrates better consistency with in situ data, exhibiting relatively higher R^2 values, 61% of evaluation pixels have R^2 values greater than 0.2 for SMAP, compared to only 20% for CYGNSS. These findings are in line with expectations, as large R^2 values are more likely to occur in regions where the SMAP data exhibits higher values in comparison to ground measurements, as evidenced by the distribution of the R^2 between SMAP and CYGNSS. However, it is observed that some regions show declining R^2 values the ground measurements. This may be attributed to the factors such as developed water systems in southern China, vegetation density, and increased urbanization, which make CYGNSS observations more vulnerable to the influence of small inland water bodies and structures. It is important to note that the CI for R^2 depends on its magnitude and is not centered on the

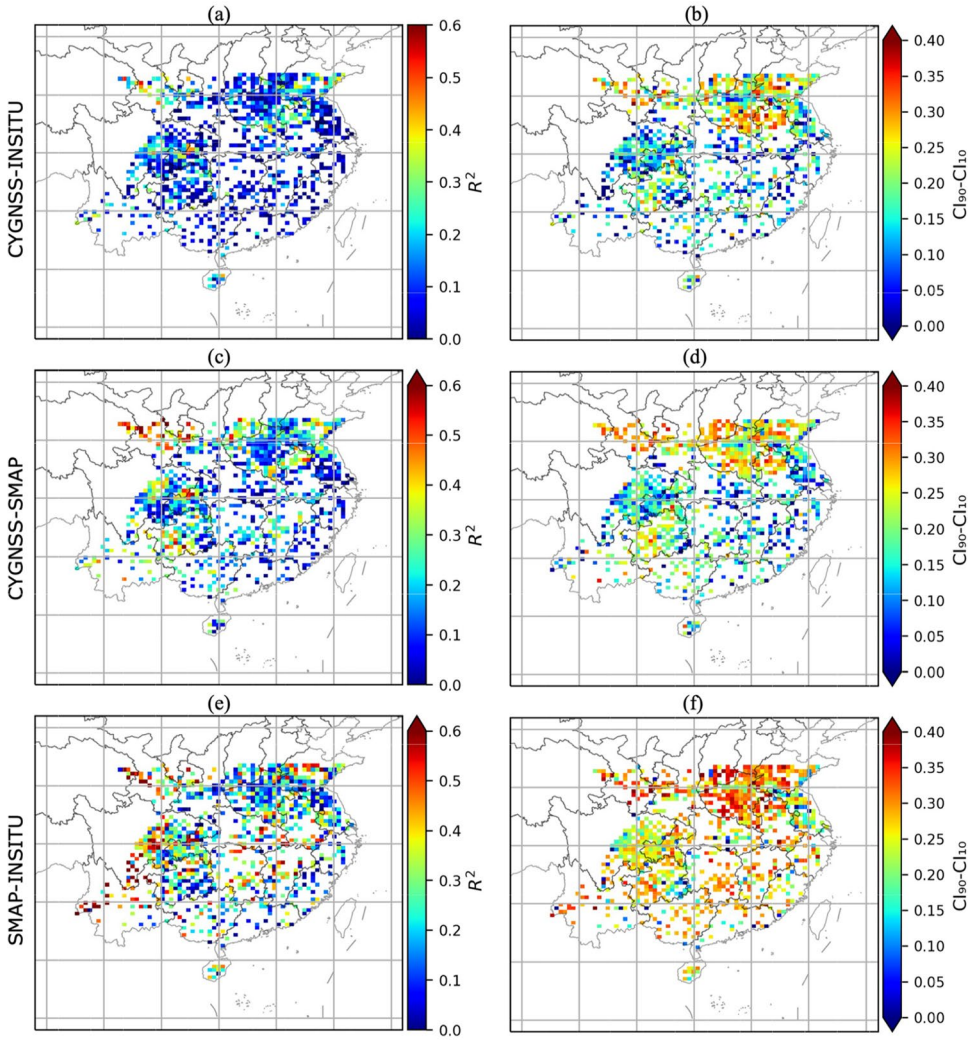

Fig. 4 Temporal coefficient of determination (**a**, **c**, **e**) and corresponding 80% confidence interval (**b**, **d**, **f**) between the raw soil moisture time series of CYGNSS, SMAP, and in situ data at collocated grid pixels

estimate itself (Gruber et al. 2020). As a result, regions with higher R^2 values exhibit larger CIs.

Figure 5 illustrates the spatial distribution of ubRMSD between CYGNSS, SMAP, and in situ data across each grid cell, accompanied by the corresponding 80% CI. The spatial map reveals that the largest ubRMSD values of both CYGNSS and SMAP, compared to in situ data, are concentrated in the Sichuan Basin, Guizhou province, Henan province, and the northern part of Anhui Province. Moreover, the magnitudes and spatial distribution characteristics of ubRMSD for two data products are similar, with slightly poorer performance observed in some limited areas for CYGNSS. Notably, the ubRMSD calculated between CYGNSS and SMAP data exhibits similar characteristics as the comparison between SMAP and in situ data. This suggests that the uncertainty of CYGNSS products primarily stems from the calibration process using reference SMAP data. Since the errors of CYGNSS-derived SSM calibrated from SMAP data are also concentrated in these areas, it results in increased ubRMSD values when evaluating CYGNSS SSM against in situ data. Consequently, this indicates that the CYGNSS SSM retrieval algorithm effectively calibrates the CYGNSS-derived effective reflectivity to SSM, affirming the potential of satellite-based GNSS-R for land remote sensing applications. It is worth mentioning that the CI also varies based on the magnitude of ubRMSD and demonstrates a similar distribution for three-group comparison.

Despite the relatively short length of the matched time series, the raw time series underwent decomposition to remove the influence of seasonal signals. A 35-day sliding average window was applied to obtain short-term anomalies, which capture individual drying and wetting events and serve as a measure of the dataset's ability to capture these variations. The skill of the SSM anomalies time series, from which the mean seasonal cycle is removed, is depicted in Figs. 6 and 7. Overall, the SMAP SSM estimates exhibit better performance in terms of R^2 and ubRMSD values compared to CYGNSS, which is consistent with the results obtained from the raw time series. Furthermore, the spatial distribution pattern of the anomalies assessment metric

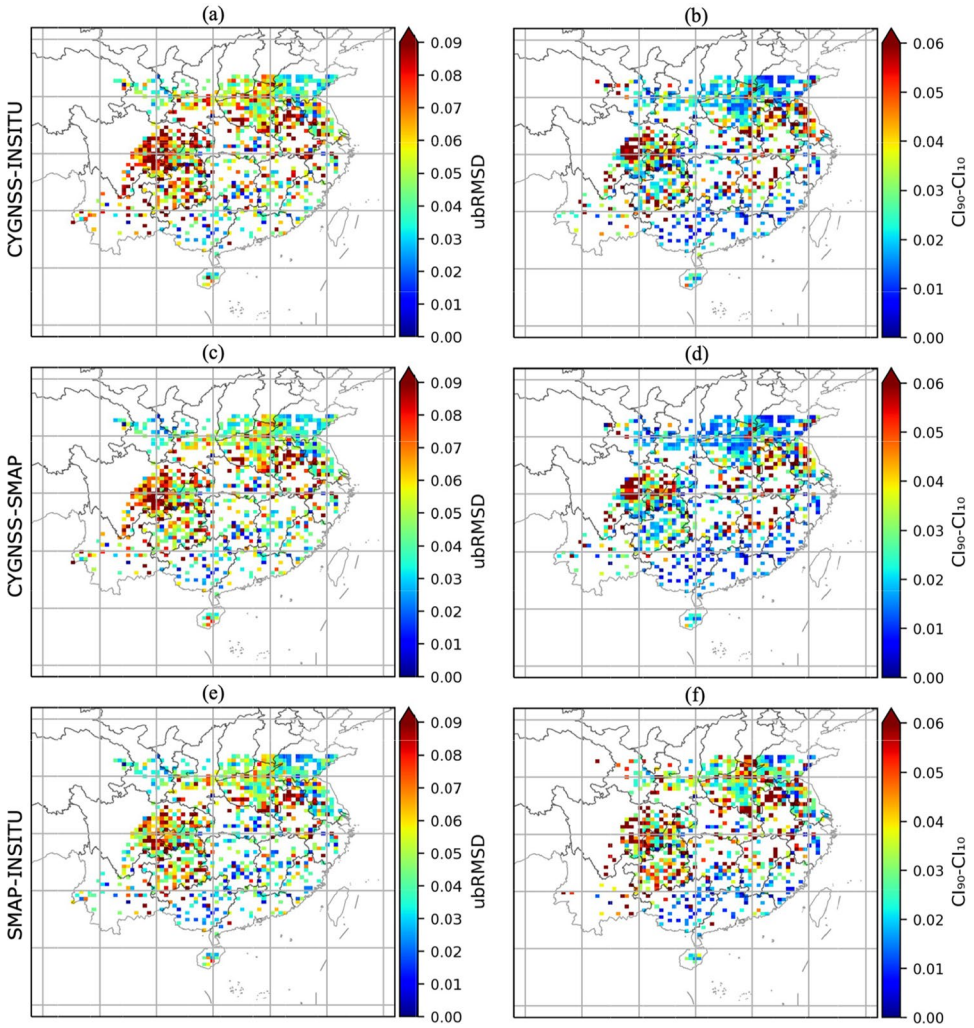

Fig. 5 Temporal ubRMSD (**a**, **c**, **e**) and corresponding 80% confidence interval (**b**, **d**, **f**) between raw soil moisture time series of CYGNSS, SMAP, and in situ data at collocated grid pixels

closely resembles that of the raw time series, except that the ubRMSD values are lower.

A boxplot in Fig. 8 provides a summary of the spatial median and interquartile range for the skill metrics, with whiskers representing the 5th and 95th percentiles. The difference between the first and third quartiles in the figure serves as an indicator of data dispersion. Additionally, Table 2 presents the summary statistics of median bias, median R^2, and median ubRMSD for daily CYGNSS, SMAP, and in-site data, allowing for further comparison. With regard to the temporal values of in situ SSM, SMAP outperforms CYGNSS significantly, which was expected given that CYGNSS SSM relies on SMAP data as the reference values in its inversion algorithm. The median bias, median R^2, and median ubRMSD between CYGNSS and in situ data are -0.016 cm^3cm^{-3}, 0.088, and 0.057 cm^3cm^{-3}, respectively. For SMAP and in situ data, the corresponding values are 0.037 cm^3cm^{-3}, 0.250, and 0.046 cm^3cm^{-3}. The variation in the estimation for both CYGNSS (80% CI=0.046, 0.075) and SMAP (80% CI=0.036, 0.070) is comparable. These results align well with previous validation studies, such as Ayres et al. (2021), Chew and Small (2018), Al-Khaldi et al. (2019), and Dong and Jin (2021), confirming the accuracy of our data preprocessing and metric calculation. When comparing the relative metrics calculated from the raw time series, the R^2 and ubRMSD values of short-anomalies time series are lower due to the removal of the seasonal cycle through sliding averaging. However, CYGNSS still exhibits considerable uncertainty in its estimates.

3.2 TCA-based evaluation results

In TCA-based evaluation, it is necessary for the errors in soil moisture time series to be independent from each other. However, as the errors of CYGNSS and SMAP SSM data are expected to be correlated, a model-based MERRA-2 SSM product was adopted. Consequently, all four data sources, including CYGNSS, SMAP, MERRA-2, and in situ data, were utilized in the TCA to estimate their random errors.

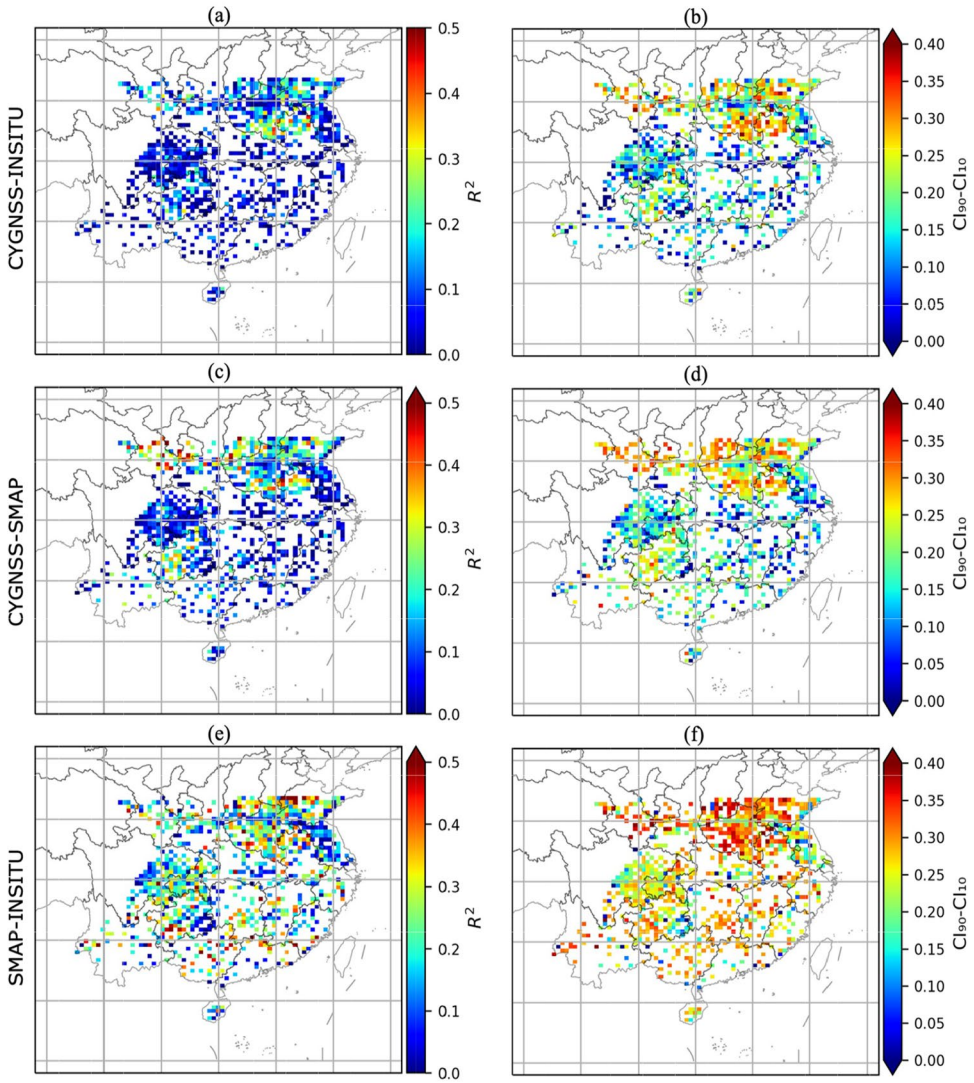

Fig. 6 Temporal coefficient of determination (**a**, **c**, **e**) and corresponding 80% confidence interval (**b**, **d**, **f**) between soil moisture anomalies of CYGNSS, SMAP, and in situ data at collocated grid pixels

Two independent data set triplets, CYGNSS-MERRA2-INSITU and SMAP-MERRA2-INSITU, were constructed. In both cases, the in situ data were employed as reference values. Additionally, the skill estimates of MERRA-2 data are collected in both sets and averaged to enhance the accuracy of the results.

Furthermore, in order to conduct the TCA-based evaluation, each triple time series of the grid required a minimum of 100 data points. After the collocation processing, only 300 grid pixels met the requirement, as the number of data pairs obtained decreased with the increasing number of collocated data sources. For each data point on the grid pixel, a skill estimate was generated using bootstrapped sampling, which provides more reliable results compared to direct estimates. And the 80% CI are provided for corresponding skill.

Figures 9 and 10 display the spatial map of TCA-based R^2 and the ESD, respectively. The spatial maps reveal distinct performance patterns among the evaluated datasets. Specifically, the TCA-based analysis reveals that SMAP and MERRA-2 exhibit satisfactory performance, while CYGNSS demonstrates the poorest performance. Across the majority of evaluated grid pixels, SMAP and MERRA-2 display higher R^2 values, with MERRA-2 slightly outperforming SMAP. In terms of the R^2, generally CYGNSS consistently exhibits the lowest median value, whereas SMAP and MERRA-2 data values consistently exceed 0.5. This trend is also observed in the ESD analysis. These findings suggest that the current version of the CYGNSS product contains greater interference information compared to SMAP and MERRA-2. Given the similarity in spatial distribution characteristics of the bootstrapped TCA error metrics of short-term anomalies, the spatial map of the short-term anomalies is omitted from the manuscript. However, summary statistics for the short-term anomalies are provided in Fig. 11 and Table 3, alongside the TCA-based estimates of the original time series, for comparative analysis.

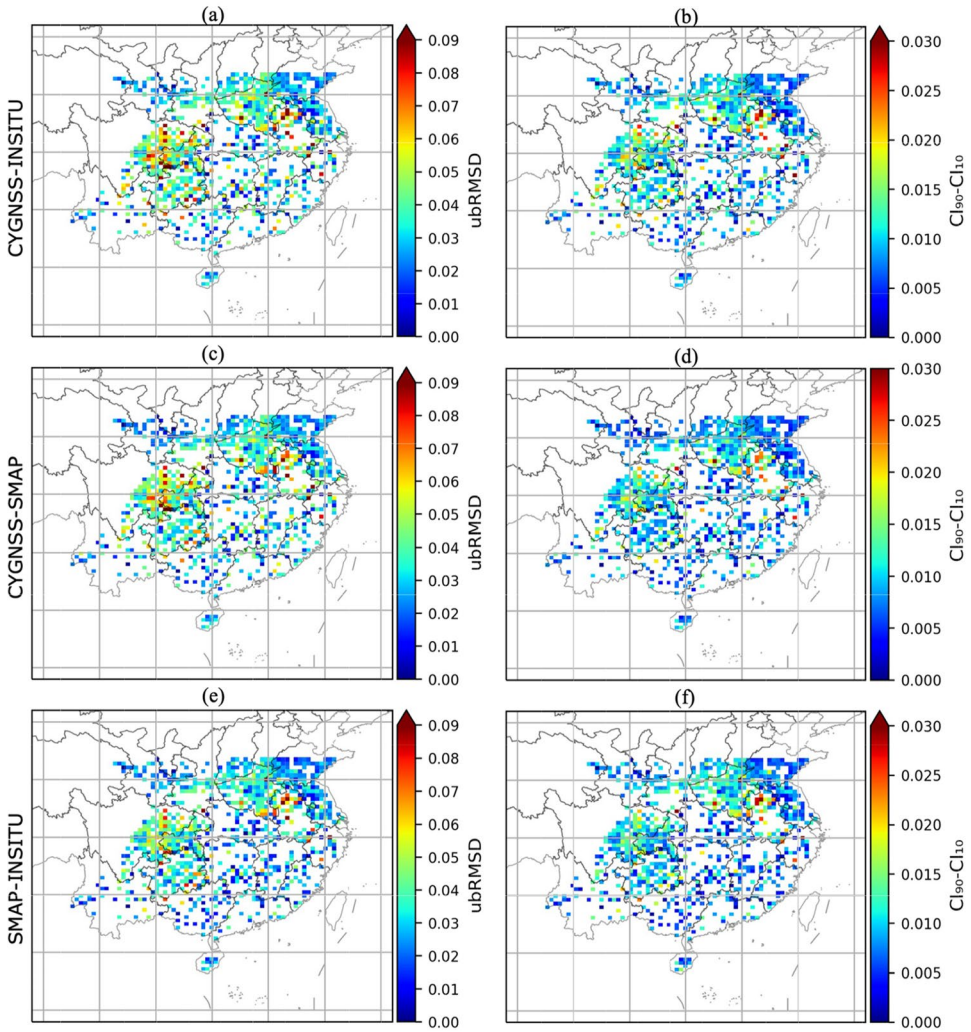

Fig. 7 Temporal ubRMSD (**a**, **c**, **e**) and corresponding 80% confidence interval (**b**, **d**, **f**) between soil moisture anomalies of CYGNSS, SMAP, and in situ data at collocated grid pixels

Figure 11 displays the median values, interquartile range, and whiskers representing the 5th and 95th percentiles of the bootstrapped TCA-based error metrics for all grid pixels. For a further comparison, Table 3 provides a comparative overview of the R^2 and ESD values, along with the corresponding 10% and 90% confidence limits. Considering the R^2 values into for both raw time series and short-term anomalies, CYGNSS consistently exhibits poorer performance compared to SMAP and MERRA-2, and MERRA-2 is superior to SMAP. Notably, the median R^2 value for raw CYGNSS data is 0.167, which is approximately three times less than that of SMAP (0.529) and MERRA-2 (0.563). Furthermore, the performance gap between CYGNSS and other two datasets widen even further for short-term anomalies. In terms of ESD, the median ESD for CYGNSS SSM is 0.055 cm^3cm^{-3}, as indicated by the statistics, whereas SMAP and MERRA-2 have lower median ESD values of 0.020 cm^3cm^{-3} and 0.021 cm^3cm^{-3}, respectively. The range of ESD values for CYGNSS is wider than that of the other datasets. Similar to the raw data, CYGNSS anomalies exhibit the highest median ESD of 0.046 cm^3cm^{-3}, compared to 0.017 cm^3cm^{-3} for SMAP and 0.012 cm^3cm^{-3} for MERRA-2, as well as a higher interquartile range and confidence bounds than the other two products. Overall, MERRA-2 slightly outperforms SMAP, while the current CYGNSS SSM shows the poorest performance among the three datasets.

4 Discussion

The accuracy of SSM products derived from spaceborne GNSS-R and understanding the spatial and temporal distribution of product uncertainty are essential for future applications and advancements in retrieval algorithm development. In addition to the quantitative evaluation discussed earlier, Fig. 12 presents the collocated SSM time series of the two representative grid pixels. One of these pixels, indexed as 95238 (latitude: 30.966°, longitude: 106.245°), has the largest data pairs among the evaluated pixels and associated with two in-situ stations. The second site, indexed as 82728 (latitude: 35.335°, longitude:

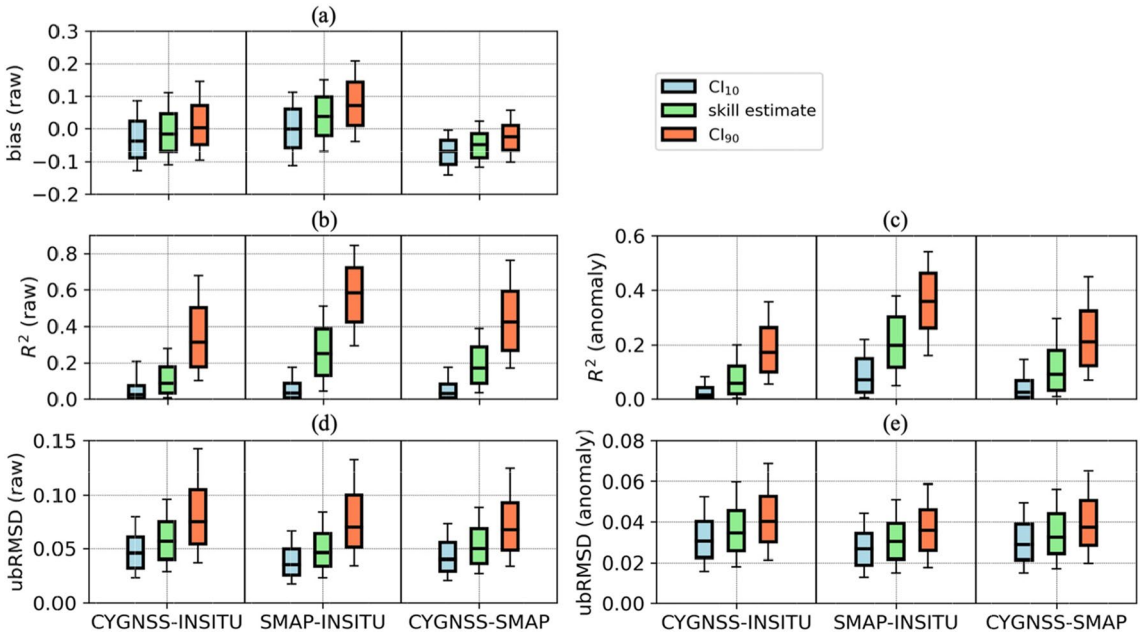

Fig. 8 Spatial summary statistics of bias [cm^3cm^{-3}] (**a**), coefficient of determination (**b**, **c**), and ubRMSDs [cm^3cm^{-3}] (**d**, **e**), along with corresponding 10% and 90% confidence limits, for raw soil moisture samples (**a**, **b**, **d**) and anomalies (**c**, **e**) of CYGNSS, SMAP, and in situ data

Table 2 The summary of the median of relative skill metrics and confidence interval limits (unit of bias and ubRMSD: cm^3cm^{-3})

Metric median	Raw			Anomalies		
	CYGNSS-INSITU	SMAP-INSITU	CYGNSS-SMAP	CYGNSS-INSITU	SMAP-INSITU	CYGNSS-SMAP
Bias CI_{10}	−0.038	−0.001	−0.069	/	/	/
Bias	−0.016	0.037	−0.048	/	/	/
Bias CI_{90}	0.003	0.071	−0.025	/	/	/
R^2 CI_{10}	0.024	0.032	0.030	0.014	0.071	0.025
R^2	0.088	0.250	0.170	0.059	0.197	0.091
R^2 CI_{90}	0.314	0.584	0.423	0.172	0.358	0.211
ubRMSD CI_{10}	0.046	0.036	0.040	0.030	0.027	0.029
ubRMSD	0.057	0.046	0.050	0.035	0.030	0.032
ubRMSD CI_{90}	0.075	0.070	0.068	0.040	0.036	0.037

114.461°), includes 10 ground stations, and its density is comparable to that of the core validation stations deployed specifically for active and passive satellite-based missions. During the summer in southern China, precipitation shows a significant increase due to the influence of the southeast monsoon originating from the low-latitude Pacific. This period is characterized as "hot and rainy period." The in situ measurements accurately capture this phenomenon, with the observed SSM displaying substantial fluctuations through the summer, as presented in Fig. 12. Comparing the results, SMAP and MERRA-2 exhibit closer agreement with the in situ SSM for the grid pixel indexed as 95238, whereas the CYGNSS product demonstrates a relatively smooth profile with minor fluctuations. This smoothness limits the ability of the CYGNSS product to accurately capture the SSM variations over the course of a year. Upon manually examination of grids with significant errors, it was discovered that CYGNSS sometimes fail to properly represent actual SSM changes. Future research should focus on investigating the underlying causes of this phenomenon, which may include factors such as the number of observations per grid pixel, representation errors, presence of inland water bodies, surface vegetation, surface roughness, and other related factors. Meanwhile, CYGNSS also demonstrates the ability to accurately capture the temporal variation of SSM at numerous

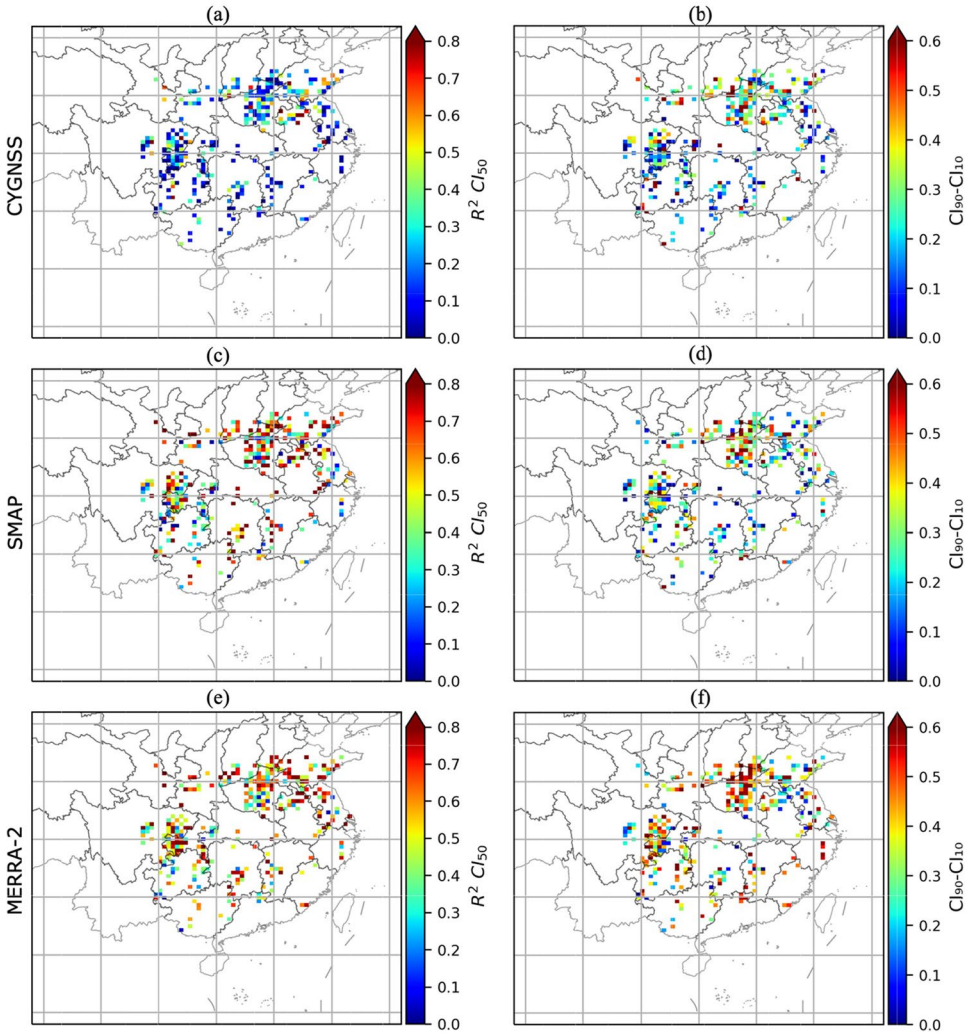

Fig. 9 Median of the bootstrapped TCA-based coefficient of determination (**a**, **c**, **e**) and corresponding 80% confidence interval (**b**, **d**, **f**) between raw soil moisture of CYGNSS, SMAP, and MERRA-2 products at the collocated grid pixel

stations, providing valuable dynamic information. This is evident in the grid pixel indexed as 82728 displayed at the bottom of Fig. 12. However, we observed significant distribution differences in the CYGNSS estimates, ranging from 0.16 to 0.24 cm^3cm^{-3}, when compared to the in situ measurements and SMAP data. These anomalies are illustrated in the scatter density plot in Fig. 13 and were not present in previous evaluations using ISMN sites.

The accuracy of the reference data play a crucial role in the estimation of SSM using the current semi-empirical retrieval algorithm employed by the UCAR/CU team and other similar studies based on CYGNSS observations. Therefore, when calibrating GNSS-R-based SSM, it is important to select reference data sources that exhibit higher levels of accuracy. Additionally, it should be acknowledged that there is still notable distinctions between spaceborne GNSS-R and conventional passive and active satellite-based microwave remote sensing sensors. The spatial resolution of the spaceborne GNSS-R observable is considered to be higher than the reference grid and more sensitive to small inland water bodies. The southern part of China, characterized by well-developed water systems, higher levels of urbanization, and extensive vegetation cover, presents challenges in accurately capturing land surface signals. The calibrated CYGNSS SSM proxy, which is aggregated in space and time, is influenced by many factors such as topography, vegetation, surface roughness, observation noise, representative errors, and modeling errors. As a result, the uncertainty associated with the CYGNSS-derived SSM product exhibits differences compared to the SMAP product. Furthermore, it is important to note that while the ground SSM measurements are taken at a depth is 0–10 cm, the sampling depth of the L-band microwave is considered to be 0–5 cm of the top layer of soil surface (Njoku and Entekhabi 1996; Chew and Small 2018). Additionally, when the in situ measurements are matched with gridded products, mismatches can generate representative error that impact evaluation results.

SSM exhibits high spatial and temporal variability, and the satellite-based GNSS-R technique provides a cost-effective solution with high spatial and temporal resolution for

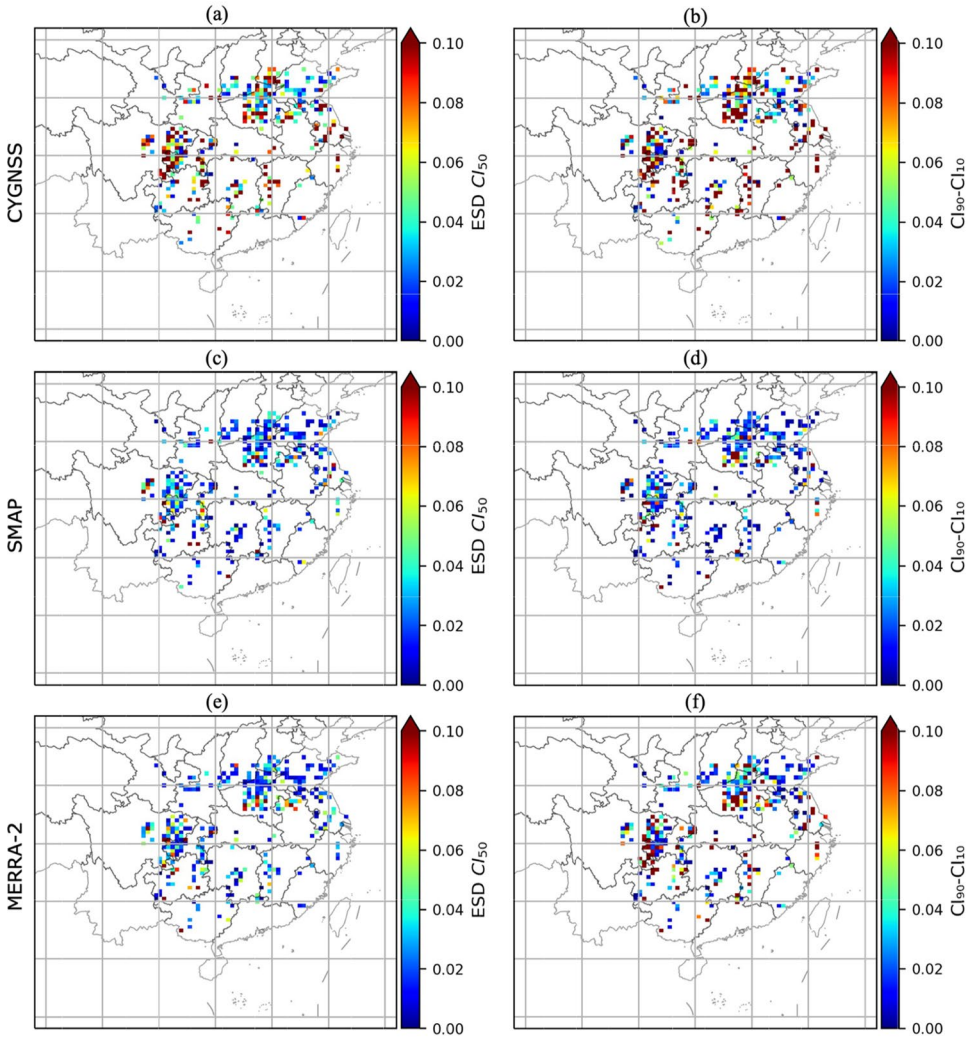

Fig. 10 Median of the bootstrapped TCA-based ESD (**a**, **c**, **e**) and corresponding 80% confidence interval (**b**, **d**, **f**) between raw soil moisture of CYGNSS, SMAP, and MERRA-2 products at the collocated grid pixel

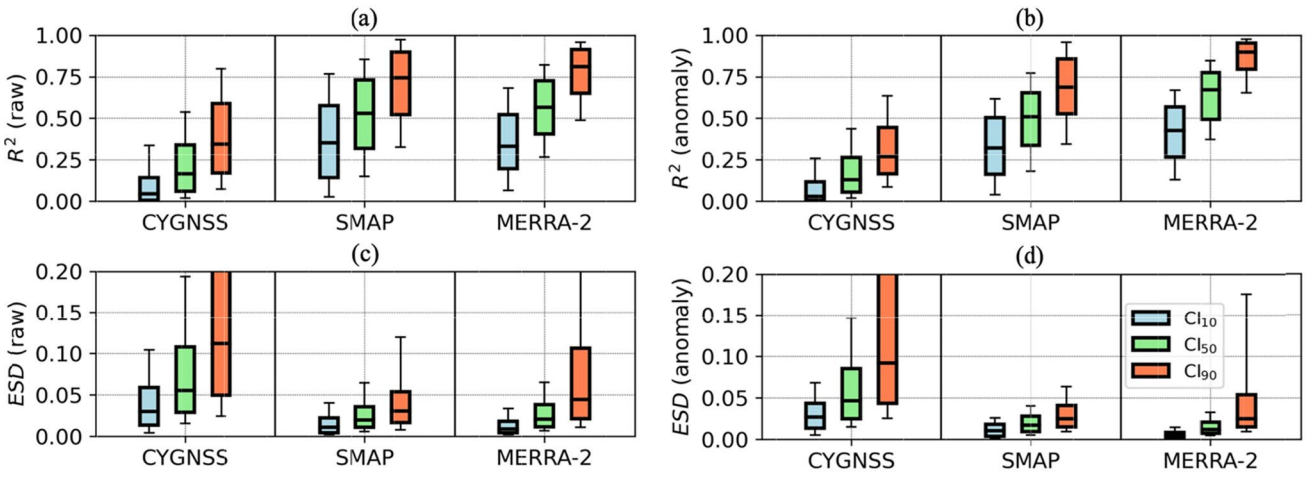

Fig. 11 Spatial summery statistics of the median of the bootstrapped TCA-based coefficient of determination (**a**, **b**) and ESD (**c**, **d**), along with corresponding 10% and 90% confidence limits, for raw soil moisture samples (**a**, **c**) and anomalies (**b**, **d**) of CYGNSS, SMAP, and in situ data

Table 3 The summary of the TCA-based metrics and confidence interval limits (unit of ESD: cm^3cm^{-3})

Metric median	Raw			Anomalies		
	CYGNSS	SMAP	MERRA-2	CYGNSS	SMAP	MERRA-2
R^2 CI_{10}	0.044	0.350	0.329	0.028	0.320	0.425
R^2 CI_{50}	0.167	0.529	0.563	0.128	0.508	0.670
R^2 CI_{90}	0.345	0.742	0.807	0.268	0.688	0.897
ESD CI_{10}	0.030	0.011	0.009	0.027	0.010	0.004
ESD CI_{50}	0.055	0.020	0.021	0.046	0.017	0.012
RSD CI_{90}	0.111	0.030	0.044	0.092	0.025	0.025

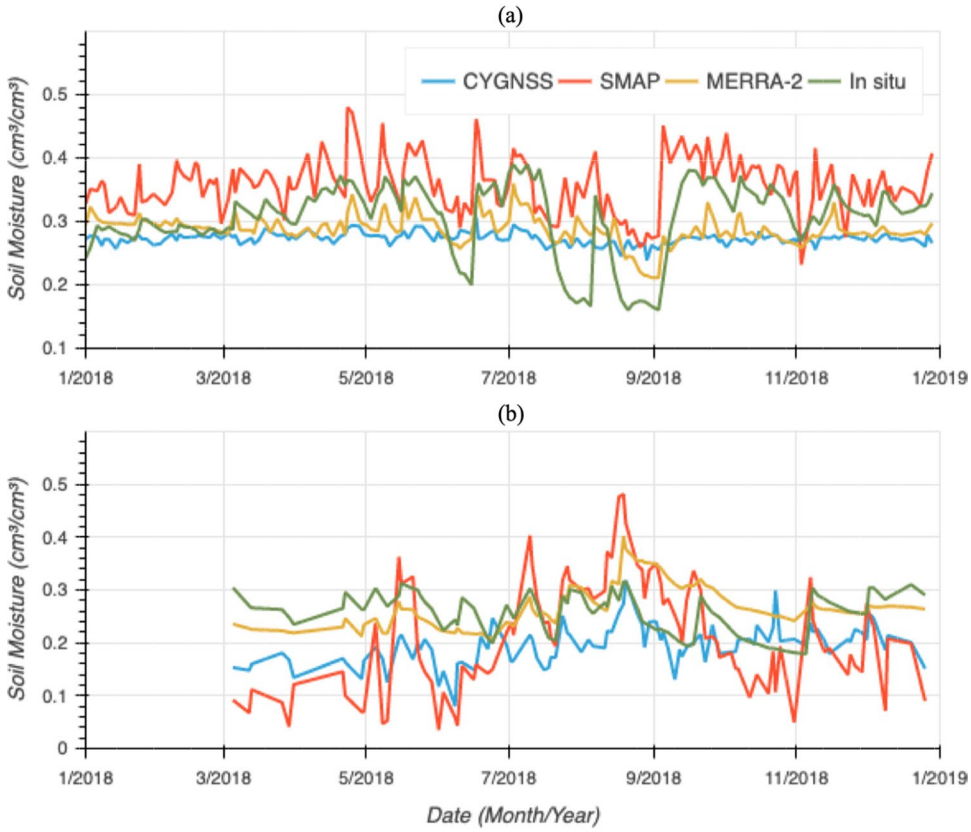

Fig. 12 Time series of different SSM for grid point indexed as 95238 including 2 in situ stations (**a**) and grid point indexed as 82728 including 10 stations (**b**)

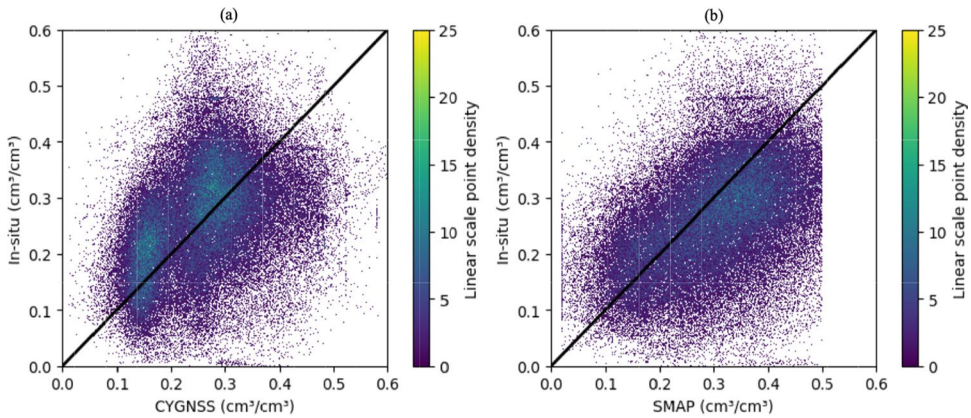

Fig. 13 Scatter density plots of collocations between CYGNSS (**a**), SMAP (**b**), and in situ data

Earth observation. However, the assessment conducted in this paper reveals that the CYGNSS SSM products suffer from significant random errors, leading to challenges in accurately capturing actual SSM changes in certain grid cells. It is important to note that the CYGNSS mission was not originally intended for land remote sensing applications. Nonetheless, the calibrated SSM product demonstrates potential in capturing the spatial and temporal dynamics of SSM. As dedicated terrestrial spaceborne GNSS-R missions are launched and retrieval algorithms continue to improve, it is expected that GNSS-R can compensate traditional satellite-based passive and active microwave remote sensing, offering wider spatial and temporal coverage for continuous Earth observation.

5 Conclusion

In order to ensure the suitability of SSM for applications in various geoscience fields, a meticulous evaluation is essential. In contrast to prior validation efforts, this study focuses on conducting a comprehensive comparison of SSM products derived from CYGNSS, aiming to quantitatively assess their uncertainty and gain insights into the current effectiveness of the spaceborne GNSS-R technique. The assessment procedure adheres strictly to recommended guidelines for evaluating satellite-based SSM products. All estimated skill metrics are accompanied by confidence intervals to provide a reliable estimation of their performance. For the first time, the performance of CYGNSS-derived SSM was assessed using in situ measurements from the Chinese soil moisture monitoring network, and the results were compared with SMAP and MERRA-2 data. The relative evaluation was conducted by comparing ground measurements from 1824 stations in southern China, which were gridded within 865 grid pixels. The analysis revealed a low R^2 value (median R^2=0.088) for the raw absolute CYGNSS SSM time series, and the ubRMSD was found to be 0.057 cm^3cm^{-3}, indicating poorer performance compared to the results obtained from SMAP against in situ measurements (median R^2=0.25, ubRMSD=0.046 cm^3cm^{-3}). Thus, the current assessment suggests that the quality of CYGNSS SSM product is inferior to that of the SMAP product. It is worth noting that the linear calibration of CYGNSS SSM proxy using SMAP SSM product in a high association between the spatial distribution features of data quality in the two datasets. The TCA demonstrates notable challenges in achieving accurate results. The evaluation based on collocated data sets collected from CYGNSS, SMAP, MERRA-2, and in situ resampled daily SSM parameter forms two groups of triples in reference to in situ measurement. The analysis exposes the presence of substantial random errors in the CYGNSS-derived SSM products within the study area. Comparatively, the skill of the MERRA-2 exhibits a slight advantage over SMAP, with both significantly outperforming CYGNSS. Nonetheless, it is important to note that CYGNSS data also performed very well in certain grid cells, effectively capturing the annual SSM changes in the corresponding region. Leveraging the continuous availability of spaceborne GNSS-R Earth Observation, the integration of SSM products ensures consistent access to high-resolution spatial and temporal information, thereby serving the needs of Earth science research. The findings presented in this study offer a comprehensive assessment of the reliability and robustness of recent released daily SSM derived from CYGNSS. Although the validations were limited to UCAR/CU published products, the results demonstrate typical characteristics and possess broad representativeness. As such, they can serve as a valuable guide for informing future algorithm development and facilitating the application of spaceborne GNSS-R SSM products.

Acknowledgements The authors would like to acknowledge the CYGNSS team and other institutions for providing the data set used in this study.

Author contributions All authors contributed to the study conception and design. Material preparation, data collection, programming development, and analysis were performed by Zhounan Dong and Shuanggen Jin. The first draft of the manuscript was written by Zhounan Dong. Li Li and Peng Wang commented on and reviewed the manuscript. All authors read and approved the final manuscript.

Funding This work was supported by National Natural Science Foundation of China (Grant number 42204014).

Data availability The CYGNSS data that support the findings of this study are freely available in the Physical Oceanography Distributed Active Archive Center (PODAAC, https://podaac.jpl.nasa.gov/datasetlist?values=CYGNSS&view=list&ids=Projects). The reference SMAP data are openly available in National Snow and Ice Data Center (NSIDC, https://nsidc.org/data/spl3smp/versions/8). The MERRA-2 data at https://gmao.gsfc.nasa.gov/reanalysis/MERRA-2/.

Code availability The code related to the manuscript will be made available from the corresponding author on reasonable request.

Declarations

Ethics approval Not applicable.

Consent to participate Not applicable.

Consent for publication Not applicable.

Conflict of interest The authors declare no competing interests.

References

Al-Khaldi MM, Johnson JT, O'Brien AJ et al (2019) Time-series retrieval of soil moisture using CYGNSS. IEEE Trans Geosci Remote Sens 57(7):4322–4331. https://doi.org/10.1109/TGRS.2018.2890646

An R, Zhang L, Wang Z et al (2016) Validation of the ESA CCI soil moisture product in China. Int J Appl Earth Obs Geoinf 48:28–36. https://doi.org/10.1016/j.jag.2015.09.009

Ayres E, Colliander A, Cosh MH et al (2021) Validation of SMAP soil moisture at terrestrial National Ecological Observatory Network (NEON) sites show potential for soil moisture retrieval in forested areas. IEEE J Sel Top Appl Earth Obs Remote Sens 14:10903–10918. https://doi.org/10.1109/JSTARS.2021.3121206

Brocca L, Melone F, Moramarco T, Morbidelli R (2010) Spatial-temporal variability of soil moisture and its estimation across scales: SOIL MOISTURE SPATIOTEMPORAL VARIABILITY. Water Resour Res 46:2. https://doi.org/10.1029/2009WR008016

Brocca L, Hasenauer S, Lacava T et al (2011) Soil moisture estimation through ASCAT and AMSR-E sensors: an intercomparison and validation study across Europe. Remote Sens Environ 115:3390–3408. https://doi.org/10.1016/j.rse.2011.08.003

Chen F, Crow WT, Bindlish R et al (2018) Global-scale evaluation of SMAP, SMOS and ASCAT soil moisture products using triple collocation. Remote Sens Environ 214:1–13. https://doi.org/10.1016/j.rse.2018.05.008

Chew CC, Small EE (2018) Soil moisture sensing using spaceborne GNSS reflections: comparison of CYGNSS reflectivity to SMAP soil moisture. Geophys Res Lett 45:4049–4057. https://doi.org/10.1029/2018GL077905

Chew C, Small E (2020) Description of the UCAR/CU soil moisture product. Remote sens 12:1558. https://doi.org/10.3390/rs12101558

Clarizia MP, Ruf CS (2016) Wind speed retrieval algorithm for the Cyclone Global Navigation Satellite System (CYGNSS) mission. IEEE Trans Geosci Remote Sens 54:4419–4432. https://doi.org/10.1109/TGRS.2016.2541343

Clarizia MP, Pierdicca N, Costantini F, Floury N (2019) Analysis of CYGNSS data for soil moisture retrieval. IEEE J Sel Top Appl Earth Obs Remote Sens 12:2227–2235. https://doi.org/10.1109/JSTARS.2019.2895510

Colliander A, Reichle R, Crow W et al (2022) Validation of soil moisture data products from the NASA SMAP mission. IEEE J Sel Top Appl Earth Obs Remote Sens 15:364–392. https://doi.org/10.1109/JSTARS.2021.3124743

Cui C, Xu J, Zeng J et al (2017) Soil moisture mapping from satellites: an intercomparison of SMAP, SMOS, FY3B, AMSR2, and ESA CCI over two dense network regions at different spatial scales. Remote sens 10:33. https://doi.org/10.3390/rs10010033

D'Agostino RB (1971) An omnibus test of normality for moderate and large size samples. Biometrika 58:341–348. https://doi.org/10.1093/biomet/58.2.341

D'Agostino R, Pearson ES (1973) Tests for departure from normality. Empirical Results for the Distributions of b2 and Ob1. Biometrika 60:613. https://doi.org/10.2307/2335012

Dong Z, Jin S (2021) Evaluation of the land GNSS-reflected DDM coherence on soil moisture estimation from CYGNSS data. Remote sens 13:570. https://doi.org/10.3390/rs13040570

Dorigo WA, Scipal K, Parinussa RM et al (2010) Error characterisation of global active and passive microwave soil moisture data sets. Global hydrology/Uncertainty analysis

Efron B, Tibshirani R (1986) Bootstrap methods for standard errors, confidence intervals, and other measures of statistical accuracy. Statist Sci 1:54–75. https://doi.org/10.1214/ss/1177013815

Entekhabi D, Njoku EG, O'Neill PE et al (2010) The Soil Moisture Active Passive (SMAP) mission. Proc IEEE 98:704–716. https://doi.org/10.1109/JPROC.2010.2043918

Eroglu O, Kurum M, Boyd D, Gurbuz AC (2019) High spatio-temporal resolution CYGNSS soil moisture estimates using artificial neural networks. Remote sens 11:2272. https://doi.org/10.3390/rs11192272

Gelaro R, McCarty W, Suárez MJ et al (2017) The Modern-Era Retrospective Analysis for Research and Applications, Version 2 (MERRA-2). J Climate 30:5419–5454. https://doi.org/10.1175/JCLI-D-16-0758.1

Gleason S, Hodgart S, Sun Y et al (2005) Detection and processing of bistatically reflected GPS signals from low Earth orbit for the purpose of ocean remote sensing. IEEE Trans Geosci Remote Sensing 43:1229–1241. https://doi.org/10.1109/TGRS.2005.845643

Gruber A, De Lannoy G, Crow W (2019) A Monte Carlo based adaptive Kalman filtering framework for soil moisture data assimilation. Remote Sens Environ 228:105–114. https://doi.org/10.1016/j.rse.2019.04.003

Gruber A, De Lannoy G, Albergel C et al (2020) Validation practices for satellite soil moisture retrievals: what are (the) errors? Remote Sens Environ 244:111806. https://doi.org/10.1016/j.rse.2020.111806

Hazra A (2017) Using the confidence interval confidently. J Thorac Dis 9:4124–4129. https://doi.org/10.21037/jtd.2017.09.14

Jia Y, Jin S, Chen H et al (2021) Temporal-spatial soil moisture estimation from CYGNSS using machine learning regression with a preclassification approach. IEEE J Sel Top Appl Earth Obs Remote Sens 14:4879–4893. https://doi.org/10.1109/JSTARS.2021.3076470

Kerr YH, Waldteufel P, Wigneron J-P et al (2010) The SMOS mission: new tool for monitoring key elements of the global water cycle. Proc IEEE 98:666–687. https://doi.org/10.1109/JPROC.2010.2043032

Martin-Neira M, Caparrini M, Font-Rossello J et al (2001) The PARIS concept: an experimental demonstration of sea surface altimetry using GPS reflected signals. IEEE Trans Geosci Remote Sens 39:142–150. https://doi.org/10.1109/36.898676

Njoku EG, Entekhabi D (1996) Passive microwave remote sensing of soil moisture. J Hydrol 184:101–129. https://doi.org/10.1016/0022-1694(95)02970-2

O'Neill PE, Chan S, Njoku EG, Jackson T, Bindlish R, Chaubell J (2021) L3 Radiometer Global Daily 36 km EASE-Grid Soil Moisture, Version 8. NASA National Snow and Ice Data Center, Boulder, Colorado USA. https://doi.org/10.5067/OMHVSRGFX38O

Peischl S, Walker JP, Rüdiger C et al (2012) The AACES field experiments: SMOS calibration and validation across the Murrumbidgee River catchment. Hydrol Earth Syst Sci 16:1697–1708. https://doi.org/10.5194/hess-16-1697-2012

Reichle RH, Draper CS, Liu Q et al (2017) Assessment of MERRA-2 land surface hydrology estimates. J Climate 30:2937–2960. https://doi.org/10.1175/JCLI-D-16-0720.1

Ruf CS, Gleason S, Jelenak Z et al (2012) The CYGNSS nanosatellite constellation hurricane mission. In: 2012 IEEE International Geoscience and Remote Sensing Symposium. IEEE, Munich, Germany, pp 214–216

Saeedi M, Sharafati A, Tavakol A (2021) Evaluation of gridded soil moisture products over varied land covers, climates, and soil textures using in situ measurements: a case study of Lake Urmia Basin. Theor Appl Climatol 145:1053–1074. https://doi.org/10.1007/s00704-021-03678-x

Stoffelen A (1998) Toward the true near-surface wind speed: error modeling and calibration using triple collocation. J Geophys Res 103:7755–7766. https://doi.org/10.1029/97JC03180

Vreugdenhil M, Greimeister-Pfeil I, Preimesberger W et al (2022) Microwave remote sensing for agricultural drought monitoring: recent developments and challenges. Front Water 4:1045451. https://doi.org/10.3389/frwa.2022.1045451

Wagner W, Dorigo W, de Jeu R et al (2012) Fusion of active and passive microwave observations to create an essential climate variable data record on soil moisture. ISPRS Ann Photogramm Remote Sens Spatial Inf Sci I–7:315–321. https://doi.org/10.5194/isprsannals-I-7-315-2012

Wan W, Ji R, Liu B et al (2022) A two-step method to calibrate CYGNSS-derived land surface reflectivity for accurate soil moisture estimations. IEEE Geosci Remote Sensing Lett 19:1–5. https://doi.org/10.1109/LGRS.2020.3023650

Wang Y, Leng P, Peng J et al (2021) Global assessments of two blended microwave soil moisture products CCI and SMOPS with in-situ measurements and reanalysis data. Int J Appl Earth Obs Geoinf 94:102234. https://doi.org/10.1016/j.jag.2020.102234

Wu D, Gao T, Xue H (2016) The study of quality control for observing data of automatic soil moisture. Hans J Soil Sci 4:1–10 (in Chinese)

Yan Q, Huang W, Jin S, Jia Y (2020) Pan-tropical soil moisture mapping based on a three-layer model from CYGNSS GNSS-R data. Remote Sens Environ 247:111944. https://doi.org/10.1016/j.rse.2020.111944